


Defect states in hexagonal boron nitride: Assignments of observed properties and prediction of properties relevant to quantum computation

A. Sajid,^{1,2} Jeffrey R. Reimers,^{1,3,*} and Michael J. Ford^{1,†}

¹*School of Mathematical and Physical Sciences, University of Technology Sydney, Ultimo, New South Wales 2007, Australia*

²*Department of Physics, GC University Faisalabad, Allama Iqbal Road, 38000 Faisalabad, Pakistan*

³*International Centre for Quantum and Molecular Structures and School of Physics, Shanghai University, Shanghai 200444, China*

 (Received 24 October 2017; revised manuscript received 21 December 2017; published 1 February 2018)

Key properties of nine possible defect sites in hexagonal boron nitride (h-BN), V_N , V_N^{-1} , C_N , V_NO_{2B} , V_NN_B , V_NC_B , V_BC_N , $V_BC_NSi_N$, and $V_NC_BSi_B$, are predicted using density-functional theory and are corrected by applying results from high-level *ab initio* calculations. Observed h-BN electron-paramagnetic resonance signals at 22.4, 20.83, and 352.70 MHz are assigned to V_N , C_N , and V_NO_{2B} , respectively, while the observed photoemission at 1.95 eV is assigned to V_NC_B . Detailed consideration of the available excited states, allowed spin-orbit couplings, zero-field splitting, and optical transitions is made for the two related defects V_NC_B and V_BC_N . V_NC_B is proposed for realizing long-lived quantum memory in h-BN. V_BC_N is predicted to have a triplet ground state, implying that spin initialization by optical means is feasible and suitable optical excitations are identified, making this defect of interest for possible quantum-qubit operations.

DOI: [10.1103/PhysRevB.97.064101](https://doi.org/10.1103/PhysRevB.97.064101)

I. INTRODUCTION

Point defects in semiconductors show a rich spin and optoelectronic physics that can be exploited to fabricate qubits for quantum computing technology [1,2] as well as for single-photon sources for quantum cryptography. Currently, the negatively charged nitrogen vacancy center (N_v^{-1}) in diamond is the leading candidate not only as a single-photon source for quantum cryptography [3,4], but also as an optically coupled quantum register for scalable quantum information processing. Possible applications include those in both quantum communication [5] and in distributed quantum computation [6]. However, useful qubits can also be conceived based on other semiconducting materials. Hexagonal boron nitride (h-BN) is a wide-band-gap (~ 6 eV) two-dimensional (2D) material with the potential to host many such color centers [7–14] that are promising candidates for quantum applications.

Both unintentional occurrence of defects (e.g., vacancies) [15,16] during the preparation of single-layer h-BN and the deterministic production of defects through electron beam radiation [17] have been shown to have considerable effects on electronic and magnetic properties of h-BN. While both nitrogen (N_v) and boron (B_v) vacancies can act as paramagnetic centers in h-BN [18], electron-paramagnetic resonance (EPR) studies indicate that N_v are more important [19–24]. Two types of paramagnetic centers have been identified: (i) three-boron centers (TBCs) in which an unpaired electron interacts with three equivalent boron (B^{11}) nuclei, producing ten-line EPR spectra, and (ii) one-boron centers (OBCs) in which oxidative damage at the center forces the unpaired electron to interact with only a single B^{11} , producing four-line EPR spectra. The

TBC can be deliberately produced either by irradiation [19–21] or by carbon doping [23], but controllable h-BN oxidation to produce OBCs has not yet been achieved. Of particular interest is that carbon-doped centers can give rise to intense photoluminescence (PL) [25,26]. Although speculations based on EPR studies have been made about the form of the TBC and OBC centers [19–24], their exact nature remains uncertain.

A priori calculations using density-functional theory (DFT) can provide useful tools for the interpretation of EPR data such as observed hyperfine tensors. Indeed, such calculations have been helpful in the identification of point defects in different semiconductors by comparing the experimental and calculated hyperfine constants [27–31]. However, the nature of many ground or excited states relevant to defects and their applications are such that DFT methods deliver results of widely varying accuracy [32], meaning that great care must always be taken when this method is applied. A summary of results comparing DFT calculations to high-level *ab initio* calculations for a model defect in h-BN, V_NC_B , concludes that DFT is reliable for the triplet-state manifold but *underestimates* the stability of closed-shell singlet states by around 0.7 eV and *overestimates* the stability of open-shell singlet states by around 0.3 eV [32], meaning that open-shell singlet states are predicted to be too low in energy by the order of 1.0 eV compared to closed-shell singlet states. In the context of this work, these errors indicate that DFT should properly describe the magnetic properties of states but the nature of the ground state may not be correctly predicted. Further, we have also considered the effects of zero-point energy correction and free-energy corrections at 298 K [32], finding sizeable changes in relative state energies of up to 0.25 eV, but corrections of this magnitude remain small compared to effects of interest herein and so are neglected.

There has been little comprehensive theoretical study on the hyperfine tensors of defects in h-BN and the prospects

*jeffrey.reimers@uts.edu.au

†mike.ford@uts.edu.au

for their exploitation in quantum computation. We consider detailed models of the TBC and OBC defects in h-BN, and also propose many defect centers, particularly defects involving introduced carbon impurity atoms. Key known properties of the TBC and OBC defects are reproduced including details of their doublet ground states. Various carbon-related antisite defects are also considered in which a nitrogen or boron vacancy is accompanied by a neighboring carbon atom and/or silicon atom substitution. In particular, defects with possible ground-state conformers of triplet character are searched for a desirable feature exploitable for quantum computation. Group-theoretical analysis is used to guide how such applications could develop, suggesting directions for experimental studies. These results are combined with our recent analyses of PL properties of h-BN defects [33] to allow focus on possible quantum-qubit applications.

II. COMPUTATIONAL METHODS

Calculations are performed for periodically replicated defects in 2D h-BN nanoflakes using DFT. For calculation of total energy, electronic structure, and ground-state geometry of all the defect supercells we used version 5.3.3 of the Vienna *Ab Initio* Simulation Package (VASP) [34,35]. For accurate calculation of electron spin density close to the nuclei, the projector augmented wave method (PAW) [36,37] was applied together with a plane-wave basis set. We utilized the standard PAW projectors provided by the VASP package. Pristine single-layer h-BN was first geometrically optimized using the conventional cell and a $21 \times 21 \times 1$ Monkhorst-Pack reciprocal space grid. A large vacuum region of 30 \AA width was used to separate a single layer of h-BN from its periodic images and to ensure that interaction between periodic images is negligible. The optimized bond length of pristine h-BN is 1.452 \AA . All the defects were then realized in a $7 \times 7 \times 1$ supercell and allowed to fully relax using a plane-wave cutoff of 350 eV for a maximum force of 0.01 eV \AA^{-1} . These optimized supercells were then embedded in $10 \times 10 \times 1$ supercells using a similar method as described in Ref. [38] for minimizing the computational cost for large calculations and to ensure no interaction in plane directions for the calculation of hyperfine coupling (HF) constants. An increased plane-wave cutoff of 500 eV was used, which was sufficient to obtain a converged spin density and HF coupling constants (A_{xx}, A_{yy}, A_{zz}), where A_{xx}, A_{yy}, A_{zz} are the principle values of the HF coupling tensor. For these supercells, the Γ -point sampling of the first Brillouin zone sufficed. We have used the nonlocal Heyd-Scuseria-Ernzerhof hybrid functional (HSE06) [39,40] by taking into account the contribution of the spin polarization of the core electrons to the Fermi-contact term. This has been shown to produce accurate results for HF tensor calculation for point defects in semiconductors [28]. Zero-field splitting tensors are evaluated using the method described in Ref. [41]. For the calculation of the spin-spin contribution to the zero-field tensor, a higher cutoff energy of 600 eV and lower force tolerance of $10^{-4} \text{ eV \AA}^{-1}$ were used. Optimized geometries from VASP were used to calculate the wave-function coefficients of defect states using SIESTA [42,43].

The band gap of pristine h-BN is calculated to be 5.69 eV , which is in reasonable agreement with the experimental value [44]. It is further seen that by changing the alpha parameter (from 0.25 to 0.75) in the HSE functional, the value of the band gap for pristine h-BN increases linearly (from 5.69 to 7.85 eV). Since the exact reproduction of an experimental gap by adjustment of the alpha parameter does not guarantee the accurate prediction of defect levels, in the present study we stick with the standard value of alpha parameter of 0.25 for HSE06. The accuracy of defect levels is ensured by calibrating the individual levels against *ab initio* CCSD(T), EOMCCSD, CASPT2, and MRCI calculations for a model compound [32].

The energies of open-shell singlet states are calculated using spin relaxed calculations (“ISPIN = 2”) with equal numbers of spin-up and spin-down electrons (“NUPDOWN = 0”) using the “FERDO” and “FERWE” commands to set non-Aufbau occupancies akin to one of the degenerate spin components of an open-shell singlet state, assuming that the resulting energy is the average of the associated singlet and triplet states [45]. The resulting wave functions are spin contaminated and violate the Gunnarsson-Lundqvist theorem [46] so that the associated densities do not provide legitimate solutions to the basic equations of DFT. However, recent calibration of this procedure for one h-BN defect against *ab initio* and time-dependent DFT (TDDFT) calculations indicates that the relative energies of different open-shell states are realistically predicted but in general these states are predicted to be 1 eV too low in energy compared to closed-shell singlet states [32]. Corrections for this effect are applied using state-specific values for $V_{\text{N}C_{\text{B}}}$ (see later in Fig. 6) and generic ones for $V_{\text{B}C_{\text{N}}}$ (see later in Fig. 7).

III. RESULTS AND DISCUSSION

In this section we present all the h-BN defects studied in this work and discuss the calculated principal values of the hyperfine coupling tensor of various defects to make comparisons with the available experimental data. A general feature of the results is that all optimized structures remained planar despite the presence of significant chemical forces favoring nonplanar structures in which missing covalent bonds in defect sites are reintroduced [32]. This means that σ - π separability remains a feature of defects in h-BN, simplifying interpretation of calculated electronic and nuclear structures. Key results are summarized in Table I while expanded results are given in the Supplemental Material [47], Table S.I.

A. Three-boron center defects

Three-boron center defects are associated with the loss of a nitrogen atom from a site in h-BN, a site surrounded by three different boron atoms. They are important as they can act as activation, recombination, absorption, or photosensitivity centers [23,25,26,48]. In experiments, they have been observed to display ten-line EPR spectra [19–24] but their precise chemical nature remains unknown. We consider three possibilities: a simple neutral defect named V_{N} in which the nitrogen atom is just removed; this with an electron trapped at the vacancy site, named V_{N}^{-1} ; and this with a carbon atom replacing the nitrogen, named C_{N} .

TABLE I. The average principle values of the HF coupling tensor $(A_{xx} + A_{yy} + A_{zz})/3$, in MHz, calculated without (with) core contribution, listing the atoms with dominant spin polarization, for various ground-state (GS) defects in h-BN, as well as with the nature of a related feasible photoluminescent (PL) state and its transition energy $h\nu$.

Defect	Symm.	GS		PL		$h\nu$ (eV)	Atoms	$(A_{xx} + A_{yy} + A_{zz})/3$
		Symm.	Occupancy ^a	Symm.	Occupancy ^a			
V_N	D_{3h}	${}^2A'_2$	$(a''_2)^1(e')^0$	${}^2E'$	$(a''_2)^0(e')^1$	3.15	B ₁ -B ₃	32 (22) ^b
V_N^{-1}	D_{3h}	${}^1A'_1$	$(a''_1)^2(a''_2)^2$					
C_N	D_{3h}	${}^2A'_1$	$(a''_1)^1$				B ₁ -B ₃	-17 (-18) ^c
V_NO_{2B}	C_s	${}^2A''$	$(a''^2)(1a')^2(a'')^1$	${}^2A'$	$(a'')^2(1a')^1(a'')^2$	1.90 ^d	B ₁	554 (506) ^e
V_NN_B	C_{2v}	2B_1	$(a_1)^2(1b_1)^1(2b_1)^0$	2B_1	$(a_1)^2(1b_1)^0(2b_1)^1$	2.12 ^d	N ₁	66
V_NCB	C_{2v}	1A_1	$(2a_1)^2(1b_1)^0(2b_1)^0$	1B_1	$(2a_1)^1(1b_1)^1(2b_1)^0$	2.08 ^f		
${}^3V_NCB^g$	C_{2v}	3B_1	$(2a_1)^1(1b_1)^1(2b_1)^0$	3B_1	$(2a_1)^1(1b_1)^0(2b_1)^1$	1.58 ^f	C	473
V_BCN	C_{2v}	3B_2	$(a_2)^1(1b_1)^1(2a_1)^0$	3A_2	$(a_2)^1(1b_1)^0(2a_1)^1$	1.54	C	28
V_BCN_{SiN}	C_s	${}^2A'$	$(a'')^2(1a')^1(2a'')^0$	${}^2A'$	$(a'')^2(1a'')^0(2a'')^1$	2.03 ^d	B ₁	338
V_NCB_{SiB}	C_s	${}^2A''$	$(1a')^2(1a'')^1(2a'')^0$	${}^2A''$	$(1a'')^2(1a'')^0(2a'')^1$	0.62 ^d	Si	66

^aList of all defect orbitals within the h-BN conduction and valence bands, with their occupancy in the dominant wave function configuration.

^bIn Ref. [24], a signal is observed of magnitude $|A_{xx} + A_{yy} + A_{zz}|/3 = 22.43 \pm 1.4$ MHz that is attributed to an N_V center.

^cIn Ref. [23], a signal is observed of magnitude $|A_{xx} + A_{yy} + A_{zz}|/3 = 20.83$ MHz that is attributed to the B^{11} atoms in a C_N TBC.

^dFrom PBE calculations, see Ref. [33]; est. maximum difference to HSE06 is 0.5 eV.

^eIn Ref. [19], a signal is observed of magnitude $|A_{xx} + A_{yy} + A_{zz}|/3 = 117.06$ MHz that is attributed to an N_V^{-1} TBC, as well as a signal at 352.70 MHz attributed to an oxygen-containing V_NO_{2B} OBC.

^fHSE06 after correction based on *ab initio* results (see Figs. 6 and 7), observed value [7,54,55] of 1.95 eV.

^gThe ground state is calculated to be 1A_1 and here the results presented are for the lowest-energy triplet state, 3B_1 .

1. Negatively charged nitrogen vacancy V_N^{-1}

It has been proposed that the observed EPR ten-line signal at 117.06 MHz originates from a negatively charged nitrogen vacancy V_N^{-1} that has a triplet ground state [19]. However, our current and others' previous calculations [9] predict that V_N^{-1} has D_{3h} symmetry supporting a closed-shell singlet ground state. Table I lists this result, labeling the ground state as ${}^1A'$ as well as listing the occupancies in the dominant wave-function configuration of all orbitals found to lie in the band gap between the h-BN valence band (VB) and the conduction band (CB). In this case, only two midgap orbitals are found in which four electrons need to be distributed, giving a simple closed-shell structure expressed in terms of them as $(a''_1)^2(a''_2)^2$. All triplet states are predicted to be of much higher energy than the ground-state singlet. As DFT calculations of the type we perform have been found to underestimate the stability of closed-shell singlet states compared to triplet states [32], this result is likely to be robust. If V_N^{-1} indeed has a singlet ground state then it cannot possibly be the source of the observed EPR signal.

2. Uncharged nitrogen vacancy V_N

This defect has been previously modeled and many key properties determined [13]. In the optimized ground-state structure shown in Fig. 1(a), the three boron atoms surrounding the vacancy relax towards each other, forming a triangular structure with D_{3h} symmetry; details of the structure are given in the Supplemental Material [47], Table S.I. The distance between any two of the boron atoms surrounding the vacancy is optimized to 2.21 Å, significantly shorter than the separation of 2.51 Å found between any two N-N or B-B nearest neighbors in pristine h-BN. Such changes are expected as the

atoms surrounding the defect strive to rearrange to eliminate dangling bonds, possibly liberating a lot of energy, opposed by constraint forces coming from the surrounding material [32]. Table I shows the two defect orbitals located within the h-BN band gap, with the ground state (GS) having an electronic configuration of $(a''_2)^1(e')^0$ with ${}^2A'_2$ π -type symmetry and a net spin polarization of 1.0. The calculated spin density is shown in Fig. 1(a), its major contribution coming from the $2p_z$ orbitals of the three boron atoms surrounding the vacancy ($\approx 0.25 \mu_B$ each), with the remaining contributions arising mostly from the B and N atoms in the next coordination shell.

Significantly, the appearance of two defect orbitals in the band gap allows for the possibility of sharp optical absorption

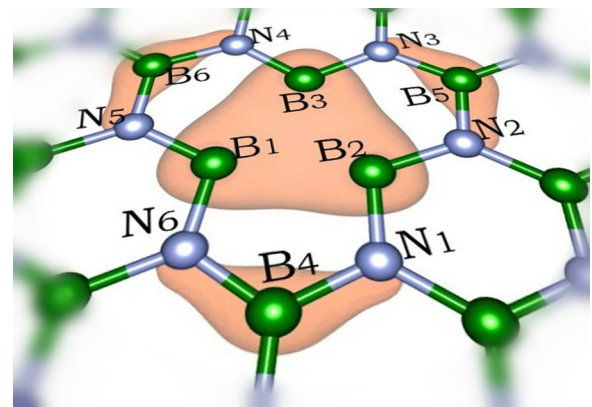


FIG. 1. Geometrical structure and isosurface of the calculated spin density for the neutral V_N center in h-BN shown from the (001) plane at isovalue $0.001 |e|/\text{Å}^3$. Spin density is concentrated on the labeled atoms, providing significant hyperfine couplings.

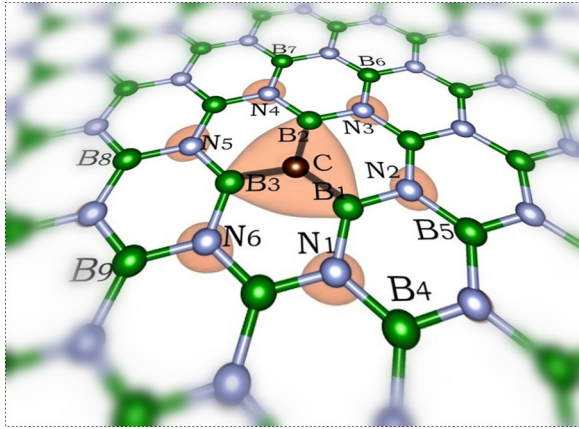


FIG. 2. Geometrical structure and isosurface of the calculated spin density for the C_N center in h-BN shown from the (001) plane at isovalue $0.001 |e|/\text{\AA}^3$. Spin density is concentrated on the labeled atoms, providing significant hyperfine couplings.

and/or emission spectra [33] involving the ground state and the ${}^2E'$ excited state, of configuration $(a''_2)^0(e')^1$; the emission energy is listed under column PL in Table I. While such transitions are symmetry forbidden, strong vibronic coupling associated with Jahn-Teller distortion could provide useful PL spectra. The calculated PL energy is 3.15 eV as listed in Table I; this value is slightly underestimated as compared with previous *GW* calculations [49] as *GW* overestimates the band gap of h-BN. However, the excited state is open shell as it contains one electron distributed among the two components of the e' orbital. This is a different type of open-shell character to that considered in our high-level *ab initio* calculations [32] and hence likely errors in this value are difficult to estimate.

Table S.I in the Supplemental Material [47] lists calculated HF coupling constants for various atoms surrounding V_N . Table I lists the average principle value $(A_{xx} + A_{yy} + A_{zz})/3$ calculated for the HF coupling tensors of the most significant atoms of the defect, B_1 – B_3 , as 32 MHz when the calculations exclude core contributions and 22 MHz when this effect is added. An h-BN defect signal has been observed in EPR spectra for the average magnitude of the principle values of the HF tensor (the Fermi-contact term) at 22.43 ± 1.4 MHz and attributed [24] to an N_V -type defect. Our calculations support this conclusion and indicate that the signal arises from the three boron-defect atoms numbered B_1 – B_3 in Fig. 1, as expected.

3. C_N center (substitutional carbon impurity)

The optimized structure for the C_N defect obtained when a carbon atom substitutes a nitrogen atom is shown in Fig. 2. The structure has D_{3h} symmetry and is very similar to pristine h-BN, with neighboring B-N bond lengths of 1.437 Å compared to 1.443 Å before substitution. The ground-state electronic structure is predicted to be ${}^2A'_1$ with, as previously predicted [9,50], only one orbital in the h-BN band gap. This state has π -type symmetry and net spin polarization of 1.0. The calculated band gap of an h-BN sheet with a C_N defect of 5.73 eV is in good agreement with previous studies [9,50]. Figure 2 shows that the unpaired spin localizes prominently on the p_z orbital of the carbon atom. Given the wide range of values that HF

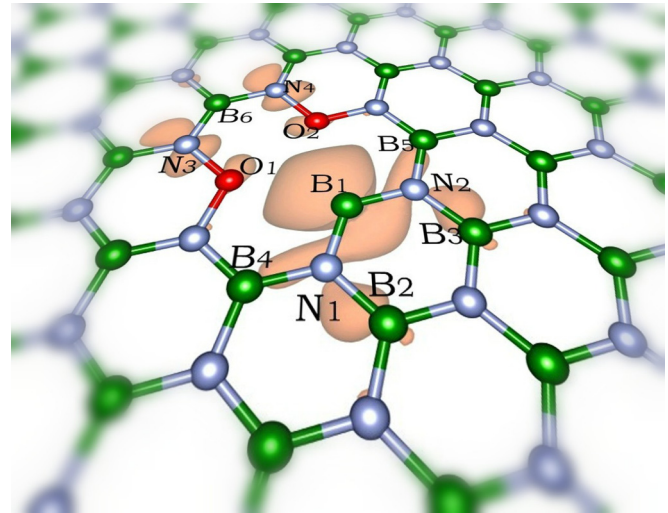


FIG. 3. Geometrical structure and isosurface of the calculated spin density for the $V_N O_{2B}$ center in h-BN shown from the (001) plane at isovalue $0.001 |e|/\text{\AA}^3$. Spin density is concentrated on the labeled atoms, providing significant hyperfine couplings.

coupling constants can take, the calculated average value of the hyperfine coupling constant of -17 MHz is close to the observed magnitude of 20.83 MHz (the sign of the HF coupling constant cannot be determined in measurements) [23] in C^{13} -enriched carbon-doped BN. As only one defect orbital lies in the band gap, sharp PL from this defect is not expected.

B. $V_N O_{2B}$ center (one-boron center defect)

Oxidation of monovacancies in h-BN has previously been studied with the aim of investigating the potential degradation of h-BN in the atmosphere and its impact on electronic and magnetic properties [18]. It has been suggested that the oxidized species provides the paramagnetic center producing observed OBC four-line EPR spectra [21,51]. To understand this effect, we consider a possible $V_N O_{2B}$ structure in which two oxygen atoms substitute boron at the defect site, making the simplest-possible oxidized OBC. The optimized structure for this defect, which has C_s symmetry, is shown along with its calculated spin density in Fig. 3. In Table I its electronic structure is reported, there being three defect orbitals in the h-BN band gap occupied by five electrons in the configuration $(a'')^2(1a')^2(2a'')^1$ to make a ${}^2A''$ ground state. In this, the unpaired electron is concentrated on atom B_1 and polarizes the oxygen atoms to give them negative hyperfine couplings. The average value of the HF coupling constant is calculated to be rather large, 506 MHz, in qualitative agreement with the observed magnitude [21] of 352.70 MHz for the OBC defect. PL from the ${}^2A''$ is expected at an energy of 1.90 eV [33].

C. Antisite defect $V_N N_B$

Nitrogen vacancies coupled with nitrogen substitution for boron on adjacent “anti” atomic sites have been proposed as a likely source of the observed intense room-temperature single-photon emission from 2D h-BN nanoflakes [7,8]. Recently, very interesting applications of spin mechanics involving

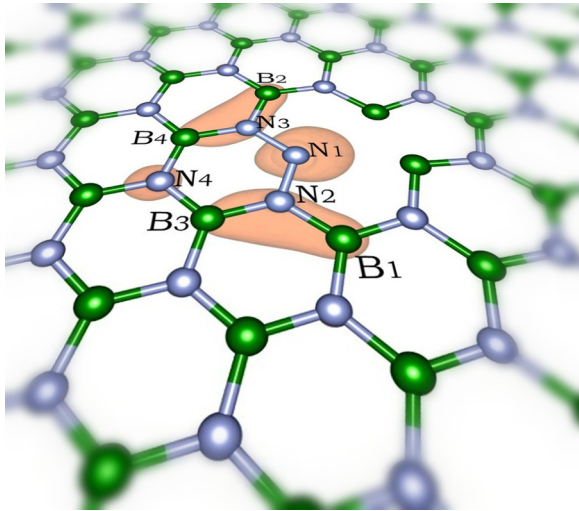


FIG. 4. Geometrical structure and isosurface of the calculated spin density for the $V_N N_B$ center in h-BN shown from the (001) plane at isovalue $0.001 |e|/\text{\AA}^3$. Spin density is concentrated on the labeled atoms, providing significant hyperfine couplings.

cooling of a mechanical resonator by coupling spin qubits with the $V_N N_B$ defect in h-BN have been proposed [52]. While no experimental EPR data are currently available for this defect, we simulate its properties so as to aid subsequent spectral assignment.

The calculated geometrical structure and spin density are shown in Fig. 4. The structure has C_{2v} symmetry with a 2B_1 π -type ground state; the unpaired electron density is localized mainly on the p_z orbital of the N_1 atom. The ground-state electronic configuration of the orbitals within the h-BN band gap is $(a_1)^2(1b_1)^1(2b_1)^0$ and the PL state also is predicted to have 2B_1 symmetry with $(a_1)^2(1b_1)^0(2b_1)^1$ configuration, as has been previously proposed [52]. PL is thus predicted to be polarized in plane along the C_{2v} axis, with calculated adiabatic transition energy 2.12 eV [33]. This is in agreement with observations and previous calculations [7].

D. Carbon- and silicon-related centers at nitrogen and boron vacancies $V_N C_B$, $V_B C_N$, $V_B C_N Si_N$, and $V_N C_B Si_B$.

While $V_N N_B$ have been directly observed [7], many related defects have been postulated [33] and here we consider the properties of some feasible defect sites. These sites are $V_N C_B$ (nitrogen vacancy with one of the surrounding borons replaced with a carbon), $V_B C_N$ (boron vacancy with one of the surrounding nitrogens replaced with a carbon), $V_N C_B Si_B$ (nitrogen vacancy with one of surrounding borons replaced with carbon and another replaced with silicon), and $V_B C_N Si_N$ (boron vacancy with one of the surrounding nitrogens replaced with carbon and another replaced with silicon). For these, optimized structures and ground-state spin densities are shown in Fig. 5. Calculated defect bond lengths are provided in the Supplemental Material [47], Table S.II, and indicate

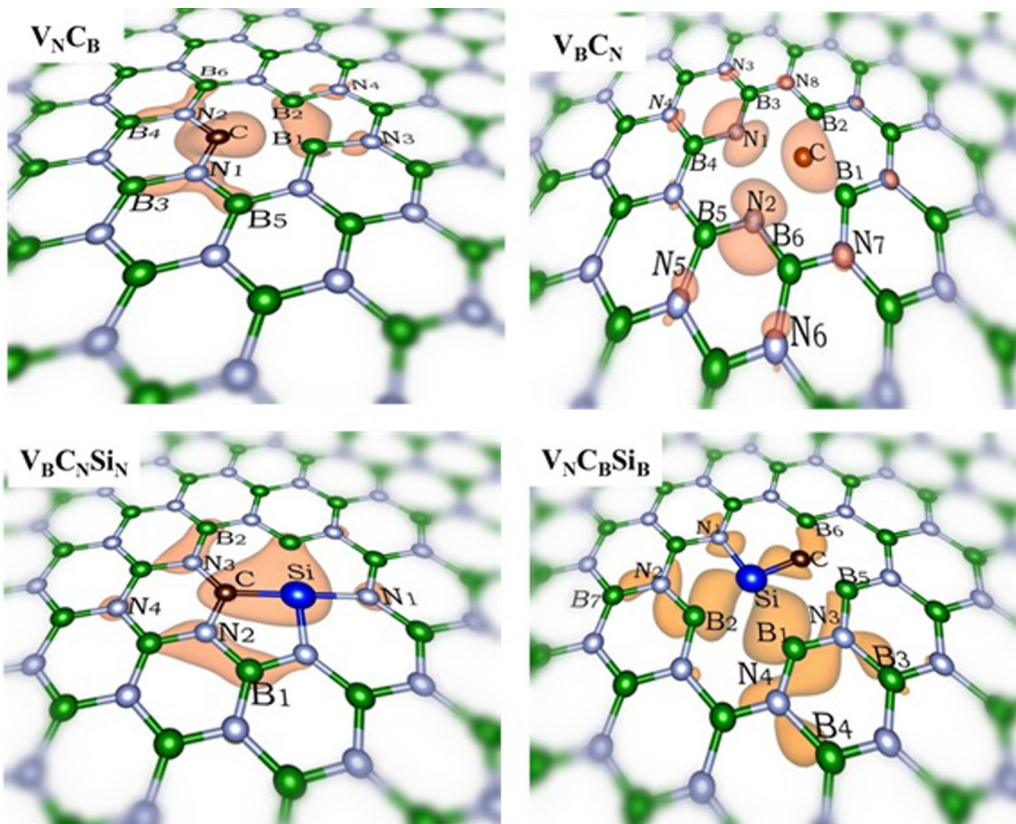


FIG. 5. Geometrical structure and isosurface of the calculated spin density for the $V_N C_B$ (isovalue $0.003 |e|/\text{\AA}^3$), $V_B C_N$ (isovalue $0.004 |e|/\text{\AA}^3$), $V_B C_N Si_N$ (isovalue $0.001 |e|/\text{\AA}^3$), and $V_N C_B Si_B$ (isovalue $0.001 |e|/\text{\AA}^3$) centers in h-BN shown from the (001) plane. Spin density is concentrated on the labeled atoms, providing significant hyperfine couplings.

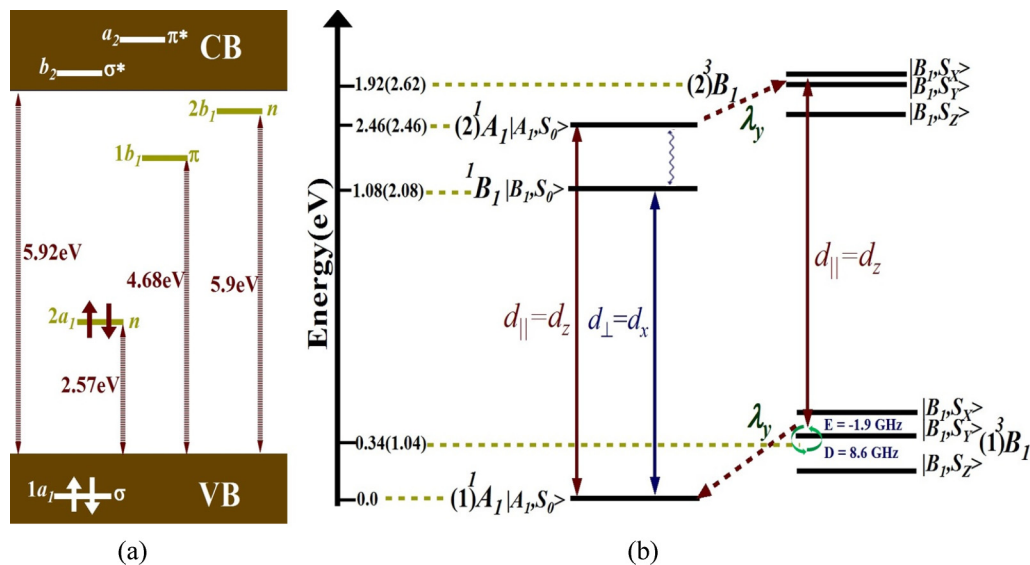


FIG. 6. (a) Key DFT orbitals from the $(1)1A_1$ closed-shell ground-state electronic structure of $V_N C_B$. The states are labeled according to the symmetry of irreducible representation as per the C_{2v} point group. The x axis is perpendicular to the plane of defect; the y, z axes are in the plane of defect. (b) HSE06 adiabatic energies of low-lying states of $V_N C_B$ as calculated by DFT, with, in (), these energies corrected according to *ab initio* CCSD(T), EOMCCSD, and CASPT2 calculations for a model compound [32]. Allowed transition polarizations d , spin-orbit couplings λ driving nonradiative transitions, and zero-field splittings are also indicated.

partial stabilization of the dangling bonds present in each defect. Calculated adiabatic transition energy, ground-state, and excited-state electronic structures are listed in Table I.

Of particular interest is the structure of $V_N C_B$ which has been previously predicted to be triplet in character [53]. However, we find the ground-state geometrical structure to be of C_{2v} symmetry and $1A_1$ in character. The properties of this defect have been the subject of recent comprehensive calculations comparing the results of DFT methods including the ones employed here to both *ab initio* calculations and various first-principles and empirical DFT calculations using model compounds to mimic the $V_N C_B$ defect [32]. These calculations indicate that the presently used method significantly *underestimates* the stability of the $1A_1$ compared to the lowest-energy triplet state, $3B_1$. Hence it is clear that the actual ground state should indeed be $1A_1$. The adiabatic energy difference between these states evaluated by DFT is 0.34 eV, but adding the correction terms found for the model compound would suggest an energy difference more like 1.04 eV. However, anticipating the possibility that a triplet state is one day observed for $V_N C_B$, results for the $3B_1$ state are also reported in Fig. 5 and Table I.

For $V_B C_N$, the ground state is calculated to be of triplet character, whereas for $V_N C_B Si_B$ and $V_B C_N Si_N$, the ground state is calculated to be doublet (see Table I). The calculated HF coupling constants for each (as well as the $3B_1$ excited state of $V_N C_B$) are given in Table I and the Supplemental Material [47], Table S.II. From Fig. 5, HF constants are dominated by the spin densities which for $V_N C_B$ are found to localize on the π orbitals of the carbon and neighboring atoms. For $V_B C_N$, the spin density is located mostly on carbon and nitrogen π orbitals, becoming highly delocalized for $V_B C_N Si_B$. Only for $V_B C_N Si_N$ does the spin density reside on σ orbitals, these showing some delocalization.

1. Possible photoluminescence arising from $V_N C_B$

In h-BN, a narrow emission band has been observed with a zero phonon line (ZPL) transition at 1.95 eV [7,54,55] but the origin of this emission is unclear. Based on a broad examination of possible defect sites in h-BN using DFT with the Perdew-Burke-Ernzerhof (PBE) functional, we have reasoned that $V_N C_B$ forms a likely candidate as its origin [33]. Here we consider this possibility in greater depth, performing calculations using the more advanced HSE06 functional. Also, we have previously performed *ab initio* calculations using the CCSD(T) [56,57], EOMCCSD [58,59], and CASPT2 [60] and MRCI [61] methods to calibrate HSE06 calculated energies for the states of $V_N C_B$ [32] and herein utilize the results to make realistic predictions of photoluminescence energies.

The electronic structure of $V_N C_B$ has been discussed in detail elsewhere [32,53], with the effects seen being generically characteristic of most h-BN defects. Basically at the defect site one σ and one π orbital on the two defect boron atoms and the carbon atom are left with dangling bonds. For the case of $V_N C_B$, four electrons need to be distributed in these orbitals. The three σ atomic defect orbitals combine to make molecular orbitals depicted in Fig. 6, one of an apparently “bonding” nature (named $1a_1$), one of a “nonbonding” nature (named $2a_1$), and one of an “antibonding” nature (named b_2). Similarly, the three π orbitals combine to make analogous orbitals named $1b_1, 2b_1$, and a_2 , respectively. The bonding orbitals have the shape of bonding orbitals found in, say, three-center two-electron bonds but the interatomic distances are so large that in reality no bond exists, and it is this feature that DFT methods find difficult to accurately model [32,62]. We find that $1a_1$ lies below the VB and so is always doubly occupied; $2a_1, 1b_1$, and then $2b_1$ fall in the VB-CB gap of h-BN, while a_2 and b_2 fall inside the CB. Transitions among these six orbitals dominate the spectroscopy of the defect, with transitions involving orbitals

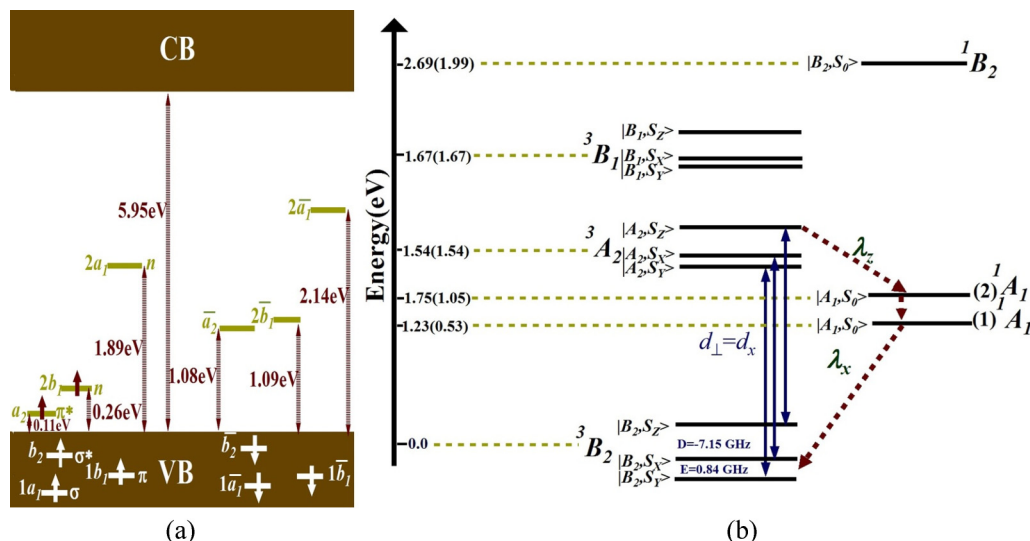


FIG. 7. (a) Key DFT orbitals from the $(1)^3B_2$ ground-state electronic structure of $V_B C_N$ (the axis conventions are the same as for $V_N C_B$). (b) HSE06 adiabatic energies of low-lying states of $V_B C_N$ as calculated by DFT, with, in (), these energies corrected according to *ab initio* CCSD(T), EOMCCSD, and CASPT2 calculations for a model compound of $V_N C_B$ [32]. Allowed transition polarizations d , spin-orbit couplings λ driving nonradiative transitions, and zero-field splittings are also indicated.

localized within the h-BN valence-conduction band gap being the most likely to produce sharp absorption and emission spectra. Visualizations of wave functions corresponding to key molecular orbitals (MOs) are shown in Fig. S.1 in the Supplemental Material [47] (mid-band-gap orbitals for the 2D layer) and elsewhere [32] (all defect orbitals for a model compound).

A search of 25 excited states of $V_N C_B$ [32] identified the only ones likely to contribute to the observed 1.95 eV photoluminescence to be $(1)^1B_1$ and $(2)^1A_1$ if the luminescence occurs within the singlet manifold, and $(1)^3B_1$ and $(2)^3B_1$ if intersystem crossing leads to population of the triplet-state manifold. These states and their properties are sketched in Fig. 6(b) and are interpreted in terms of the orbital energies for the $(1)^1A_1$ ground state shown in Fig. 6(a). The energies shown in this figure include those calculated using DFT as well as those corrected using *ab initio* calculated corrections [32]. The lowest-energy adiabatic transition within the singlet manifold is predicted to be $(1)^1B_1 \rightarrow (1)^1A_1$ at 2.08 eV, close to the observed value, while the lowest-energy transition within the triplet manifold is predicted to be a bit lower in energy, $(2)^3B_1 \rightarrow (1)^3B_1$ at 1.58 eV. The singlet-manifold transition is allowed with an oscillator strength calculated by TDDFT for a model compound to be 0.0002 [32]. By symmetry this transition will have its dipole oriented perpendicular to the plane of the h-BN layer and emission would therefore be in the plane. There is also a singlet-manifold transition with its dipole in the plane at 2.46 eV involving the doubly excited $(2)^1A_1$ state. While its dipole strength will be very small, emission with a reasonable lifetime could result following intersystem crossing to the $(1)^3B_1$ state. While the best estimate of the state energies after correction has this process endothermic by 0.16 eV, it is feasible that the reaction is exothermic instead, making it also feasible that this transition produces the observed photoemission.

2. Spin-orbit coupling and zero-field splitting in $V_N C_B$ and $V_B C_N$ defects

Since spin-orbit coupling can mix the triplet and singlet spin states, generating intersystem crossings, while spin-spin interaction lifts the degeneracy of spin multiplets, we briefly study the effect of these two interactions for $V_N C_B$ and $V_B C_N$ defects. $V_B C_N$ is chosen as it is the only defect predicted to have a triplet ground state, making it feasible for use in quantum spin devices. The electronic orbital energies of this defect are shown in Fig. 7 and are analogous to those shown in Fig. 6 for $V_N C_B$, except that the involved σ orbitals are now ordered $1a_1 < b_2 < 2a_1$ while the π orbitals are ordered $1b_1 < a_2 < 2b_1$. Its ground state is 3B_2 with the lowest-energy singlet state calculated to be 1A_1 at an adiabatic transition energy of 1.23 eV as calculated by DFT, changing to 0.53 eV applying likely corrections based on the *ab initio* calculations for $V_N C_B$. This energy difference is sufficiently high such that the prediction of a triplet ground state is likely to be robust. For $V_B C_N$, three defect orbitals (see the Supplemental Material [47], Fig. S1) fall within the VB of h-BN, making them doubly occupied, while the remaining three orbitals fall in the band gap between VB and CB and are occupied by two electrons. We also consider spin-orbit coupling in $V_N C_B$ owing to its somewhat analogous electronic structure and its low-lying triplet state that could be made accessible.

The characteristics of the spin-orbit interactions [63], zero-field splitting, and allowed intersystem crossing and optical transitions are complex; these are discussed in detail in the Supplemental Material [47], Sections S2–S4, respectively. A summary of the results is presented in Figs. 6 and 7 highlighting the allowed in-plane and out-of-plane transitions, corresponding HSE06 adiabatic energies of these transitions, and the possible paths of relaxation to the ground state. The key conclusion reached is that through appropriate optical pumping

and relaxation cycles, ground-triplet-state spin polarization can be achieved for $V_B C_N$ defect in h-BN, making it of possible use in quantum information devices [64–66]. Thus we discuss in the Supplemental Material [47], Sections S2–S4, how long-lived quantum memory in h-BN can be achieved for $V_N C_B$ owing to the lifetime differences of first- and second-order transitions from different triplet substates to the singlet ground state. The result for $V_B C_N$ is most significant as for this defect the triplet state is predicted to be the ground state of the system. Thus in subsequent optical cycles ground-state spin polarization can be achieved for $V_B C_N$ as intersystem crossing results in preferential filling of $m_s = \pm 1$ spin sublevels of the triplet ground state.

IV. CONCLUSIONS

The properties of nine possible defect centers in h-BN were examined, focusing on EPR properties such as the HF tensor of the ground state. This work is then related to prospective photoluminescence properties and assignments presented for a range of observed data concerning h-BN defects. Assignment is made of the observed [24] EPR signal at 22.43 MHz to V_N ,

the observed [23] signal at 20.83 MHz to C_N , the observed [19] signal at 352.70 MHz to $V_N O_{2B}$, and also tentative assignment of the observed photoemission 0-0 transition at 1.95 eV to $V_N C_B$.

Of all the defects examined, only $V_B C_N$ was predicted to have a triplet ground state. We show that the available combination of excited-state energetics, spin-orbit coupling, and zero-field splitting parameters leads to a scenario in which ground-state spin polarization and long-lived quantum memory in h-BN can be achieved for $V_B C_N$ and $V_N C_B$, respectively, by optical means, making these defects of interest for use in quantum computation.

ACKNOWLEDGMENTS

This work was supported by resources provided by the National Computational Infrastructure (NCI), and Pawsey Supercomputing Centre with funding from the Australian Government and the Government of Western Australia. A.S. acknowledges receipt of an Australian Postgraduate Award funded by Grant No. ARC DP 150103317. Funding is also acknowledged from Grant No. ARC DP 160101301 and Chinese NSF Grant No. 1167040630.

-
- [1] T. D. Ladd, F. Jelezko, R. Laflamme, Y. Nakamura, C. Monroe, and J. L. O'Brien, *Nature* **464**, 45 (2010).
 - [2] D. D. Awschalom, L. C. Bassett, A. S. Dzurak, E. L. Hu, and J. R. Petta, *Science* **339**, 1174 (2013).
 - [3] R. Brouri, A. Beveratos, J.-P. Poizat, and P. Grangier, *Opt. Lett.* **25**, 1294 (2000).
 - [4] A. Beveratos, R. Brouri, T. Gacoin, A. Villing, J.-P. Poizat, and P. Grangier, *Phys. Rev. Lett.* **89**, 187901 (2002).
 - [5] L. Childress, J. M. Taylor, A. S. Sørensen, and M. D. Lukin, *Phys. Rev. Lett.* **96**, 070504 (2006).
 - [6] L. Jiang, J. M. Taylor, A. S. Sørensen, and M. D. Lukin, *Phys. Rev. A* **76**, 062323 (2007).
 - [7] T. T. Tran, K. Bray, M. J. Ford, M. Toth, and I. Aharonovich, *Nat. Nanotechnol.* **11**, 37 (2016).
 - [8] T. T. Tran, C. Elbadawi, D. Totonjian, C. J. Lobo, G. Grosso, H. Moon, D. R. Englund, M. J. Ford, I. Aharonovich, and M. Toth, *ACS Nano* **10**, 7331 (2016).
 - [9] B. Huang and H. Lee, *Phys. Rev. B* **86**, 245406 (2012).
 - [10] S. Azevedo, J. R. Kaschny, C. M. de Castilho, and F. de Brito Mota, *Nanotechnology* **18**, 495707 (2007).
 - [11] T. M. Schmidt, R. J. Baierle, P. Piquini, and A. Fazzio, *Phys. Rev. B* **67**, 113407 (2003).
 - [12] W. Orellana and H. Chacham, *Phys. Rev. B* **63**, 125205 (2001).
 - [13] M. S. Si and D. S. Xue, *Phys. Rev. B* **75**, 193409 (2007).
 - [14] R.-F. Liu and C. Cheng, *Phys. Rev. B* **76**, 014405 (2007).
 - [15] K. S. Novoselov, D. Jiang, F. Schedin, T. J. Booth, V. V. Khotkevich, S. V. Morozov, and A. K. Geim, *Proc. Natl. Acad. Sci. U.S.A.* **102**, 10451 (2005).
 - [16] O. L. Krivanek, M. F. Chisholm, V. Nicolosi, T. J. Pennycook, G. J. Corbin, N. Dellby, M. F. Murfitt, C. S. Own, Z. S. Szilagy, and M. P. Oxley, *Nature* **464**, 571 (2010).
 - [17] J. C. Meyer, A. Chuvilin, G. Algara-Siller, J. Biskupek, and U. Kaiser, *Nano Lett.* **9**, 2683 (2009).
 - [18] J.-W. Feng and J.-X. Zhao, *J. Mol. Model.* **20**, 2197 (2014).
 - [19] A. Katzir, J. Suss, A. Zunger, and A. Halperin, *Phys. Rev. B* **11**, 2370 (1975).
 - [20] A. Zunger and A. Katzir, *Phys. Rev. B* **11**, 2378 (1975).
 - [21] E. Andrei, A. Katzir, and J. Suss, *Phys. Rev. B* **13**, 2831 (1976).
 - [22] D. Geist and G. Römelt, *Solid State Commun.* **2**, 149 (1964).
 - [23] A. Moore and L. Singer, *J. Phys. Chem. Solids* **33**, 343 (1972).
 - [24] M. Fanciulli and T. D. Moustakas, in *Wide Band Gap Semiconductors*, Proceedings of the Annual Fall Meeting of the Materials Research Society (Materials Research Society, Pittsburgh, PA, 1992).
 - [25] M. G. Silly, P. Jaffrennou, J. Barjon, J.-S. Lauret, F. Ducastelle, A. Loiseau, E. Obraztsova, B. Attal-Tretout, and E. Rosencher, *Phys. Rev. B* **75**, 085205 (2007).
 - [26] L. Ci, L. Song, C. Jin, D. Jariwala, D. Wu, Y. Li, A. Srivastava, Z. F. Wang, K. Storr, L. Balicas *et al.*, *Nat. Mater.* **9**, 430 (2010).
 - [27] A. Gali, M. Fyta, and E. Kaxiras, *Phys. Rev. B* **77**, 155206 (2008).
 - [28] K. Szász, T. Hornos, M. Marsman, and A. Gali, *Phys. Rev. B* **88**, 075202 (2013).
 - [29] K. Szász, X. T. Trinh, N. T. Son, E. Janzén, and A. Gali, *J. Appl. Phys.* **115**, 073705 (2014).
 - [30] K. Szász, V. Ivády, I. A. Abrikosov, E. Janzén, M. Bockstedte, and A. Gali, *Phys. Rev. B* **91**, 121201 (2015).
 - [31] J. C. C. Freitas, W. L. Scopel, W. S. Paz, L. V. Bernardes, F. E. Cunha-Filho, C. Speglich, F. M. Araújo-Moreira, D. Pelc, T. Cvitanić, and M. Požek, *Sci. Rep.* **5**, 14761 (2015).
 - [32] J. Reimers, R. A. Sajid, and M. J. Ford (unpublished).
 - [33] S. A. Tawfik, S. Ali, M. Fronzi, M. Kianinia, T. T. Tran, C. Stampfl, I. Aharonovich, M. Toth, and M. J. Ford, *Nanoscale* **9**, 13575 (2017).
 - [34] G. Kresse and J. Hafner, *Phys. Rev. B* **47**, 558 (1993).
 - [35] G. Kresse and J. Furthmüller, *Comput. Mater. Sci.* **6**, 15 (1996).
 - [36] P. E. Blöchl, *Phys. Rev. B* **50**, 17953 (1994).
 - [37] G. Kresse and D. Joubert, *Phys. Rev. B* **59**, 1758 (1999).

- [38] A. Alkauskas, B. B. Buckley, D. D. Awschalom, and C. G. Van de Walle, *New J. Phys.* **16**, 073026 (2014).
- [39] J. Heyd, G. E. Scuseria, and M. Ernzerhof, *J. Chem. Phys.* **118**, 8207 (2003).
- [40] A. V. Krukau, O. A. Vydrov, A. F. Izmaylov, and G. E. Scuseria, *J. Chem. Phys.* **125**, 224106 (2006).
- [41] V. Ivády, T. Simon, J. R. Maze, I. A. Abrikosov, and A. Gali, *Phys. Rev. B* **90**, 235205 (2014).
- [42] E. Artacho, E. Anglada, O. Diéguez, J. D. Gale, A. García, J. Junquera, R. M. Martin, P. Ordejón, J. M. Pruneda, D. Sánchez-Portal, and J. M. Soler, *J. Phys.: Condens. Matter* **20**, 064208 (2008).
- [43] J. M. Soler, E. Artacho, J. D. Gale, A. García, J. Junquera, P. Ordejón, and D. Sánchez-Portal, *J. Phys.: Condens. Matter* **14**, 2745 (2002).
- [44] G. Cassabois, P. Valvin, and B. Gil, *Nat. Photonics* **10**, 262 (2016).
- [45] U. von Barth, *Phys. Rev. A* **20**, 1693 (1979).
- [46] O. Gunnarsson and B. I. Lundqvist, *Phys. Rev. B* **13**, 4274 (1976).
- [47] See Supplemental Material at <http://link.aps.org/supplemental/10.1103/PhysRevB.97.064101> for a complete table of calculated principle values of HF tensor and detailed discussion of spin-orbit and spin-spin interactions.
- [48] S. N. Grinyaev, F. V. Konusov, V. Lopatin, and L. N. Shiyani, *Phys. Solid State* **46**, 435 (2004).
- [49] C. Attaccalite, M. Bockstedte, A. Marini, A. Rubio, and L. Wirtz, *Phys. Rev. B* **83**, 144115 (2011).
- [50] N. Berseneva, A. Gulans, A. V. Krasheninnikov, and R. M. Nieminen, *Phys. Rev. B* **87**, 035404 (2013).
- [51] A. Reinberg, *J. Chem. Phys.* **41**, 850 (1964).
- [52] M. Abdi, M.-J. Hwang, M. Aghtar, and M. B. Plenio, *Phys. Rev. Lett.* **119**, 233602 (2017).
- [53] G. D. Cheng, Y. G. Zhang, L. Yan, H. F. Huang, Q. Huang, Y. X. Song, Y. Chen, and Z. Tang, *Comput. Mater. Sci.* **129**, 247 (2017).
- [54] R. Bourrellier, S. Meuret, A. Tararan, O. Stéphan, M. Kociak, L. H. Tizei, and A. Zobelli, *Nano Lett.* **16**, 4317 (2016).
- [55] L. J. Martínez, T. Pelini, V. Waselowski, J. R. Maze, B. Gil, G. Cassabois, and V. Jacques, *Phys. Rev. B* **94**, 121405 (2016).
- [56] G. P. Purvis III and R. J. Bartlett, *J. Chem. Phys.* **76**, 1910 (1982).
- [57] K. Raghavachari, G. W. Trucks, J. A. Pople, and M. Head-Gordon, *Chem. Phys. Lett.* **157**, 479 (1989).
- [58] J. F. Stanton and R. J. Bartlett, *J. Chem. Phys.* **98**, 7029 (1993).
- [59] T. Korona and H.-J. Werner, *J. Chem. Phys.* **118**, 3006 (2003).
- [60] K. Andersson, P.-Å. Malmqvist, and B. O. Roos, *J. Chem. Phys.* **96**, 1218 (1992).
- [61] K. R. Shamasundar, G. Knizia, and H.-J. Werner, *J. Chem. Phys.* **135**, 054101 (2011).
- [62] Z.-L. Cai and J. R. Reimers, *J. Chem. Phys.* **112**, 527 (2000).
- [63] M. Tinkham, *Group Theory and Quantum Mechanics* (Dover, Mineola, NY, 2003).
- [64] F. J. Heremans, C. G. Yale, and D. D. Awschalom, *Proc. IEEE* **104**, 2009 (2016).
- [65] D. Lee, K. W. Lee, J. V. Cady, P. Ovarthaiyapong, and A. C. B. Jayich, *J. Opt.* **19**, 033001 (2017).
- [66] P. Udvarhelyi, G. Thiering, E. Londero, and A. Gali, *Phys. Rev. B* **96**, 155211 (2017).